Design and Fabrication of Nanopillar Patterned Au Textures for Improving Nanotribological Performance

Wenjie Zhao,[†,‡] Liping Wang,[*,†] and Qunji Xue[†]

State Key Laboratory of Solid Lubrication, Lanzhou Institute of Chemical Physics, Chinese Academy of Sciences, Lanzhou 730000, China, and Graduate School of Chinese Academy of Sciences, Beijing 100039, China

ABSTRACT Fast development of micro/nanoelectromechanical systems (MEMS/NEMS) and high-density storage technology (HDT) have stimulated the development of new materials that require hydrophobic surfaces with low adhesion and friction. Micro/nanohierarchical structures and chemical modification are two useful methods for improving nanotribological properties of mechanical components. In this study, Au surfaces with micro/nanohierarchical structures were prepared by replication of micropatterened silicon surfaces using PDMS and self-assembly of alkanethiol [$CH_3(CH_2)_9SH$] to create hydrophobic micro/nanohierarchical structures and to improve nanotribological properties of MEMS/NEMS. The effects of nanoscaled roughness (including pillar height and pillar fractional surface coverage) and chemical modification on the wetting and nanotribological properties of surfaces were systemically investigated. Results show that with the increasing of nanoscale roughness and lowering of surface energy, the surface becomes more hydrophobic, and the adhesive force and friction force are reduced greatly.

KEYWORDS: pillar • SAMs • height and fractional surface coverage • nanotribological performance • MEMS/NEMS

1. INTRODUCTION

Functional surfaces with micro/nanohierarchical textures have attracted the increasing interest of researchers from materials science and nanoscience because of their great advantages in applications such as hydrophobic, antiadhesion, and friction-reduction etc. (1–6), for example, lotus leaf show self-cleaning function that contaminations can be easily moved from the surface and water striders can stand effortlessly on water because their legs are composed of numerous needle-shaped setae with diameters on micro scale and that each micro seta is composed of many elaborate nano scale grooves.

The surfaces in MEMS/NEMS and HDT are generally separated by a couple of nanometers (7, 8). Surface forces such as Van der Waals, capillary, electrostatic, and chemical bonding forces become significant compared with body force (gravity and normal load) as the size of devices shrinks to micro- and nanoscales, and then adhesion, stiction, and friction are the major factors that cause the failure of MEMS/NEMS (8–10).

In general, two important factors need to be taken into consideration in order to create a superhydrophobic or nonadhesive surface (11–14). First, the surface should be roughened. Second, the surface should have low surface energy (in other words, it should be hydrophobic). For the first factor, it is usually to control surface roughness by changing the height and fractional surface coverage of micro/nano- hierarchical textures. For the second factor, surface energy is determined by surface chemistry, which chemically modified with SAMs. The motivation for these improvements for MEMS/NEMS is to increase the density of components, to lower their cost, and to enhance their performance per device/integrated circuit.

Surface textures and chemical modification are commonly used in magnetic disk drives and MEMS/NEMS to reduce friction and adhesion in order to reduce the possibility of mechanical failure (15–18). A number of fabrication methods were used to generate micro/nanohierarchical structures, including laser/plasma/chemical etching (19), soft photolithography (20), sol−gel processing and solution casting (21), electrical/chemical reaction and deposition (6), microcontact printing (22), AFM local anodic oxidation (23), and so on. However, there are several limitations of these conventional approaches when applied to practical industry, such as high capital and operating costs, specific material limitation, complication, and so on, and so none of them can be considered as an ideal and generally acceptable tool.

Replica molding has been developed in the past decade and is a relatively inexpensive, convenient, high efficiency, and more importantly, environmentally friendly route toward accurate patterning of various materials (6, 22, 24). In this article, Au surfaces patterned with pillars of varying height and fractional surface coverage were fabricated by replication of Si micropattern template with different surface morphology and then chemically modified with hydrophobic alkanethiol. The fabrication technique used here is a low-cost, two-step process, which provides flexibility in fabrication of various hierarchical structures. The surface micro/

* Corresponding author. Tel: +86 931 4968080. Fax: +86 931 4968163. E-mail: lpwang@licp.cas.cn.

Received for review November 14, 2009 and accepted February 15, 2010

† Lanzhou Institute of Chemical Physics, Chinese Academy of Sciences.

‡ Graduate School of Chinese Academy of Sciences.

DOI: 10.1021/am900788t

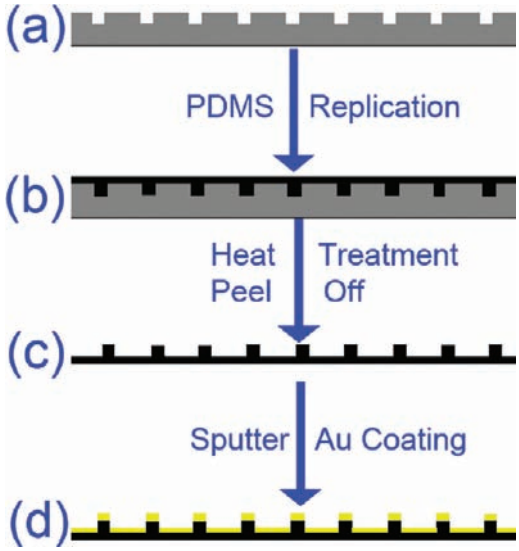

FIGURE 1. Schematic process flow of the replication procedure for fabricating Au patterned surfaces with micro/nano pillars.

nanohierarchical structures can be tailored by adjusting the depth and fractional surface coverage of cylinder hole. Ultrathin SAMs as molecular-level protective/lubrication coatings are commonly used in HDT and MEMS/NEMS for improving wetting, adhesion, friction, and corrosion problems (25). In this work, SAMs of octadecanethiol (ODT) was used to control chemical and physical properties of Au interface.

An AFM tip that slides on a silicon surface is a suitable model system for the sliding behavior in MEMS/NEMS and magnetic disks because the nanotextures tend to dominate the contact condition as compared to the AFM tip (2, 9, 26, 27). In this work, various micro/nanotexture Au surfaces with different pillar height and pillar fractional surface coverage were generated via micromolding technique and chemically modified with ODT SAMs. A comprehensive study of the nanoscale friction and adhesion properties with various nanotextures was present. The aim of this investigation was to further improve the knowledge of the relations between surface texture, surface chemistry, and nanotribological properties. It is expected that this investigation could help to understand and aid the design and selection of appropriate nanopatten parameters for MEMS/NEMS.

2. EXPERIMENTAL SECTION

PDMS prepolymer (Sylgard 184 Silicone Elastomer Kit, Dow Corning, Midland, MI, USA) was purchased from USA. Octadecanethiol (ODT) was purchased from Aldrich, 98%. Both acetone and anhydrous ethanol were analytical reagents. All reagents were used as received.

The method used to fabricate various micro/nanotexture Au surfaces is cheaper, simple and reproducible. The schematic process flow to create micro/nanometersized Au pillars with different height and area density is shown in Figure 1. (a) The process began with a Si P(100) substrate template with different depth and area density cylinder hole textures, which are depicted in Figure 2. Before being used, the micro/nanopatterned silicon master was cleaned with acetone, ethanol, and distilled water consequently in an ultrasonic bath. (b) A curing agent and the PDMS prepolymer were thoroughly mixed in a 1:10 weight ratio. After 10 min of manual mixing, the prepolymer mixture was degassed in a desiccator at room temperature for about 3 h to remove any air bubbles in the mixture to ensure complete mixing of the two parts. The PDMS was spin-coated on the Si template, followed by heat treated at 70 °C for 10 h with a vacuum oven. (c) PDMS was peeled from the Si template when it solidified completely. The negative surface texture of the original template was transferred to the PDMS film. (d) At last, samples were sputter-coated with a thin layer of gold (100 nm).

The patterned Au surfaces were placed in a 5 mMol/L anhydrous ethanol solution of ODT for 24 h at room temperature. Samples were taken from the ODT solution and put in an oven maintained at 70 °C for 3 h. The samples were then washed with sufficient anhydrous ethanol to remove the physical adsorbed molecules and dried under a flow of N_2.

The static water contact angles on the prepared surfaces were measured according to the sessile droplet method using a drop shape analysis system (DSA100, Kruss Company Ltd., Germany) with a computer-controlled liquid dispensing system. Deionized water droplets with a volume of 5 μL were used. The contact angle was determined by fitting a Young−Laplace curve around the drop. The experiment was performed under normal laboratory ambient conditions, 20 °C, and 30% relative humidity. The mean value was calculated from at least 10 individual measurements and the measurement error was less than 3°.

A PHI-5702 multifunctional X-ray photoelectron spectroscope (XPS) was used to determine the chemical states of some typical elements in the Au surface and surface modified with ODT SAMs, using Mg Ka radiation as the excitation source, at a pass energy of 29.35 eV and a resolution of ± 0.3 eV; the binding energy of contaminated carbon (C1s: 284.8 eV) was used as reference.

Atomic force microscopy (AFM) is a suitable technique for surface morphology, friction and wear characterization at the nanoscale as it has the ability to measure material properties with high spatial resolution (26, 27). Nanofriction force and adhesion force was measured experimentally by an AFM/FFM (CSPM4000, Benyuan, China), using the contact mode. Commercially available rotated monolithic silicon probe, symmetric tip shape (Budget Sensors, Multi75Al-G-10, 30 nm thick Aluminum coating) with a nominal spring constant of 3 N/m and a coated tip with a curvature radius of less than 10 nm was employed. Details of the technique have been described elsewhere (10, 23). Friction forces were obtained from friction-load line at 100 separate points on each surface with a scan frequency of 1 Hz and a scan size of 60 × 60 μm^2. The output voltages were directly used as frictional forces. No attempt was made to calibrate the torsion force constant. Repeated measurements were within 1% of the average value for each sample.

Adhesive force (F) which is also called pull-off force were got from force−distance curve, and was calculated by the following equation (28, 29)

$$F = K_c Z_p$$

Where K_c is the force constant of cantilever and Z_p is the vertical displacement of the piezotube. For all measurements, the same tip was used in this study. All the measurements were performed at room temperature with a relatively humidity of 30−40%. Repeated measurements were within 5% of the average value for each sample.

3. RESULTS AND DISCUSSION

3.1. Surface Morphology. 2D, 3D, and line cross-section analysis AFM topographic images of Si templates and

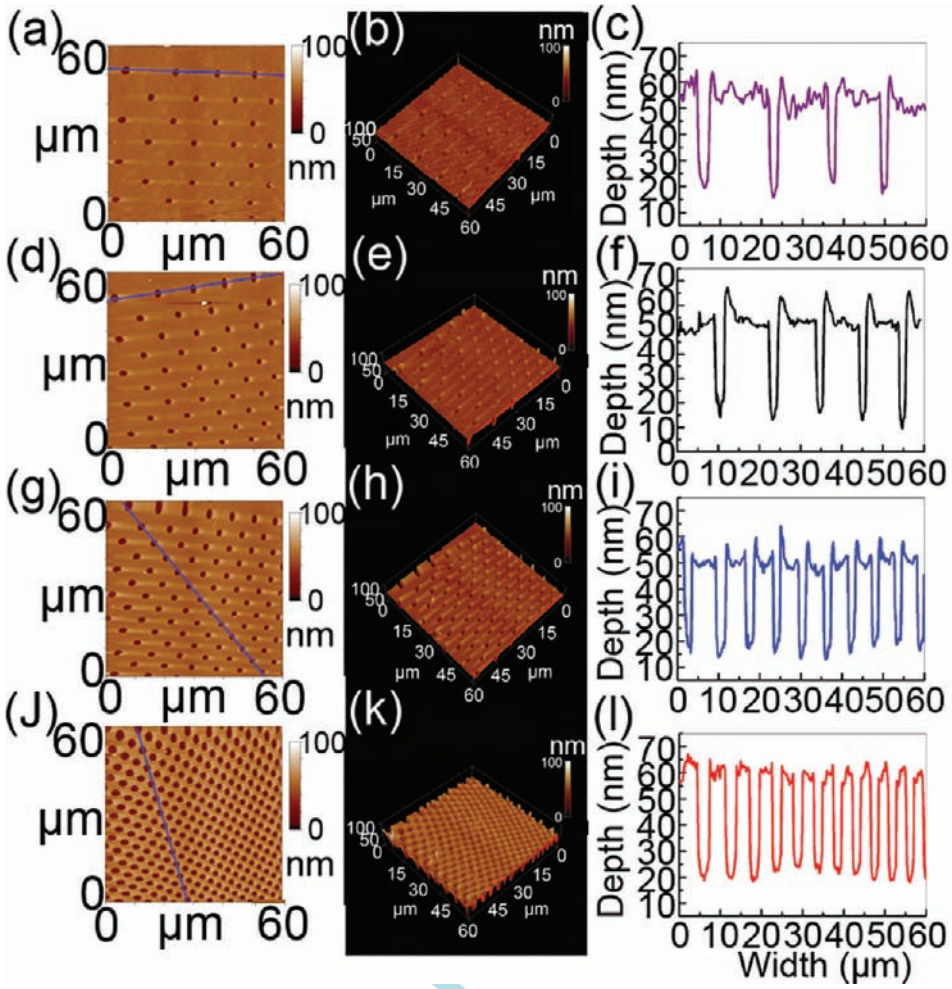

FIGURE 2. Surface topographies of Si templates used in this work.

micro/nanopattern Au surfaces were depicted in Figure 2 and Figure 3. As seen form Figure 2, the Si micro/nanohole textures with the same depth but varying fractional surface coverage were clearly shown. As depicted in Figure 3, Au micro/nanopillars were fabricated successfully that have the same height (20 nm) and diameter (2 μm) but different area density. For convenience, we ascribe the micro/nanotexture Au surface as P and micro/nanotexture Au surface chemically modified with ODT SAMs as P-HS, respectively. We abbreviate nanotexture surface with the different cylindrical pillar fractional surface coverage from low to high as P-1, P-2, P-3, and P-4. We also abbreviate nanotexture surface with different height as PA (20 nm) and PB (40 nm). Correspondingly, Au surfaces with micro/nanotexture from low area density to high area density and from low to tall height chemically treated by ODT SAMs are ascribed to PHS-A1, PHS-A2, PHS-A3, PHS-A4, PHS-B1, PHS-B2, PHS-B3, and PHS-B4, respectively.

Figure 4 shows the schematic process flow for geometrical parameters of Au micro/nanopillars. The pattern is a there-dimensional array of cylinder pillars. The critical parameters are the diameter of each cylinder pillar (d), the interval distance between adjacent cylinder pillars (i), and the height of each cylinder pillar (h). Roughness in terms of rms was determined by the analysis software of the AFM and the pillar-to-pillar distance found by analysis of cross-section lines was taken in different directions from the images. Repeated measurements were within 5% of the average value for each sample.

Pillar fractional surface coverage r (%) was determined by the following equation:

$$r(\%) = NS_{\text{pillar}}/S_{\text{scan}} = N\pi R^2/S_{\text{scan}}$$

where N is the number of pillar; R is the radius of pillar; S_{scan}= the AFM scan area.

According to the above calculation, the pillar fractional surface coverage r (%) from low to high is 3.5, 4.9, 9.3, and 27.8%, respectively. All geometrical parameters including the height, diameter, fractional surface coverage, and surface roughness are summarized in Table 1. As seen from Table 1, surface roughness increased as the pillar height and fractional surface coverage increased.

3.2. XPS Investigation. To gain further insights on the chemical states of surface chemical composition, ww performed XPS investigation on all samples. Figure 5 presents XPS spectrum of micro/nanotexture Au surface with or without chemically modified with ODT SAMs. In Figure 5a, peaks of Au 4f7/2 and Au 4f5/2 appear at 84.05 and

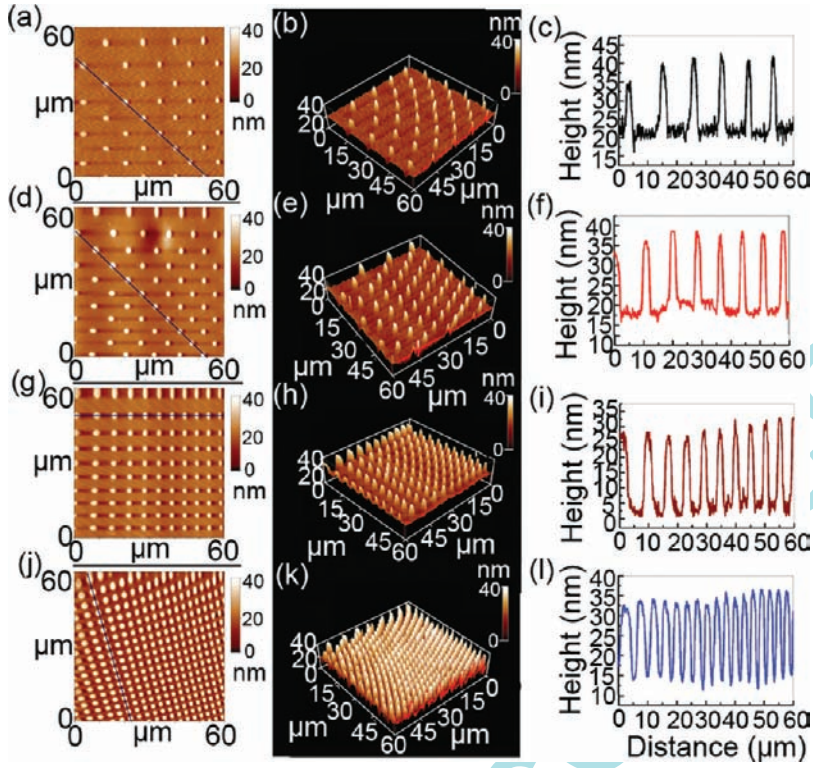

FIGURE 3. Surface morphologies of Au patterned surfaces fabricated in this work.

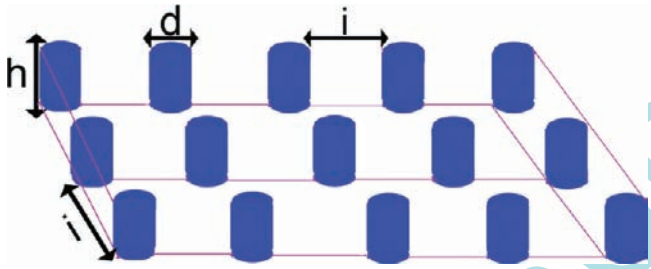

FIGURE 4. Design parameters for the Au micro/nanopillars.

87.73 eV that may correspond to that Au metal. When the Au surface was modified by ODT SAMs, the binding energy of Au 4f7/2 and Au 4f5/2 shifts a little high to 84.46 eV and 88.16 eV, respectively. This is assigned to the bonding between S atoms with Au atoms (30). It can be seen from Figure 5b that the S peak only appears when Au surface modified with ODT SAMs, which implies that ODT SAMs was successfully formed on Au texture surface. The S2p spectrum of the ODT positioned at 162.53 eV is also assigned to the bound S atoms (30). It is clearly that no additional shoulder peak on the S2p spectrum, which reveals that a uniform monolayer was formed on Au texture surface (31).

3.3. Contact Angle Measurements. Wetting/dewetting ability is an important property for a solid surface because it plays a crucial role in many industrial applications, which is determined by measuring contact angles of the water liquid droplet at equilibrium states. In our work, contact angle measurements were made for a more quantitative understanding of the effect of micro/nanostructure and chemical treatment on wetting/deweting properties. Contact angle on nonpatterned Au surface with sooth silicon surface topography was used as comparison.

Contact angles on patterned Au surfaces increase largely when compared with nonpatterned Au surfaces with (73°) or without ODT SAMs (64°). As shown in Table 2, the relationship between the surface properties and the contact angle is evident. The wettability of a solid surface depends on both the surface structure and the surface energy (1, 2, 32). Increasing of surface roughness (pillar height and fractional surface coverage) and lowering of the surface energy (chemical treatment with alkanthiol) enhances the surface hydrophobicity. This is because with the increasing surface roughness, air may be trapped in the cavities of a rough surface,

Table 1. Geometrical Parameters of Au Patterned Surfaces with Micro/Nano Pillars Used in Our Experiment

name	pillar height h (nm)	pillar diameter d (μm)	pillar interval i (μm)	surface roughness rms (nm)	pillar fractional surface coverage r (%)
P-A1	20	2	7.5	3.27	3.5
P-A2	20	2	6	3.48	4.9
P-A3	20	2	1.8	5.72	9.3
P-A4	20	2	1.6	6.47	27.8
P-B1	40	2	7.5	4.93	3.5
P-B2	40	2	6	5.53	4.9
P-B3	40	2	1.8	7.6	9.3
P-B4	40	2	1.6	11.3	27.8

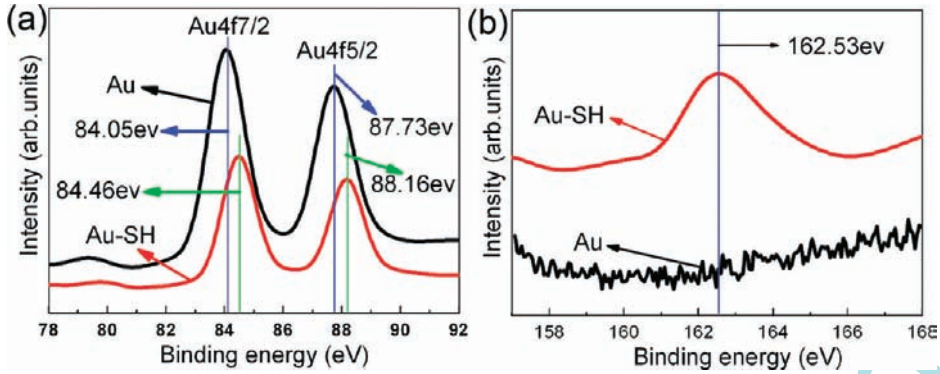

FIGURE 5. XPS spectra of (a) Au 4f7/2 and Au 4f5/2; (b) S 2p of the micro/nanotexture Au surface before and after being modified with ODT SAMs.

Table 2. Contact Angles (deg) of Au Patterned Surfaces before and after Chemical Modification

(□)	1	2	3	4
P−A	90	100	104	106
P−B	94	105	109	111
PHS−A	107	110	112	115
PHS−B	110	112	114	117

resulting in a composite solid−air−liquid interface, as opposed to the homogeneous solid−liquid interface (1, 2). And lowering surface energy with chemical treatment, ODT SAMs has terminal groups ($-CH_3$), which are hydrophobic, would lead to higher contact angle (25, 33). By controlling these factors and varying them independently, we can design suitable surface for special MEMS/NEMS application.

3.4. Adhesion Measurement. Adhesion is generally measured by the amount of force necessary to separate two surfaces in contact and the results are shown in Figure 6. It is observed that the adhesive forces are closely related to the surface coverage density and pillar height of micro/nanonanotextures, also are influenced strongly by chemical modification with ODT SAMs. As shown in Figure 6, for the adhesive force values there is a decrease when the pillar height and fractional surface coverage increases. Adhesive force also decreased greatly after chemical modification. Compared with the nonpatterned Au surface, the Au surface with micro/nanopillar textures greatly improved the adhesive properties and showed lower adhesive forces. Among the Au surfaces with micro/nanopillar textures, P-A1 with the lowest height (20 nm) and fractional surface coverage (3.5%) shows the largest adhesive force. PHS-B4 with the largest height (40 nm), fractional surface coverage (27.8%), and chemical modification with ODT SAMs shows the lowest adhesive force.

It is well-established that adhesive force is determined by two important factors: contact interfacial forces and noncontact forces such as Van der Waals, electrostatic forces and capillary/meniscus forces (1, 23, 34). At first, adhesive force is closely related to the real contact area between the tip and surface, larger area lead to bigger adhesive force. With the increase in pillar height and fractional surface coverage, the tip traveling between the pillars results in the decrease of the contact area, responsible for decreased adhesive force (34–36). Second, when the solid surfaces were hydrophilic, they would easily form meniscus by the adsorbed water molecules, thus they had larger adhesive force. However, when the surfaces were hydrophobic, they would show lower adhesion (1, 2, 10). Chemical modification with ODT SAMs increases the surface hydrophobicity of micro/nanotexture Au surfaces, which leads to the reduction of adhesion force. Therefore, surface textures and chemical modification were two useful common methods that can be used to help solve adhesion problems by reducing the real area of contact and increasing the surface hydrophobicity.

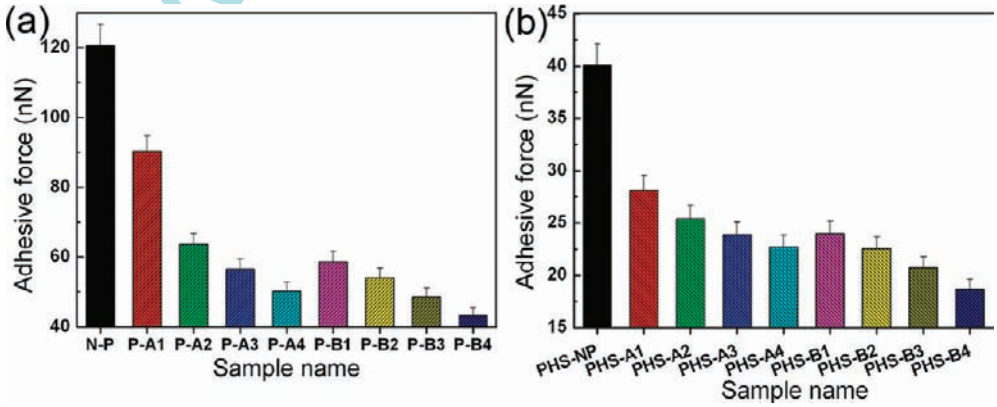

FIGURE 6. Adhesive forces between AFM tip and Au micro/nano patterned surfaces with different height and surface coverage before and after SAMs chemical modification at room temperature and a relative humidity of 30−40%.

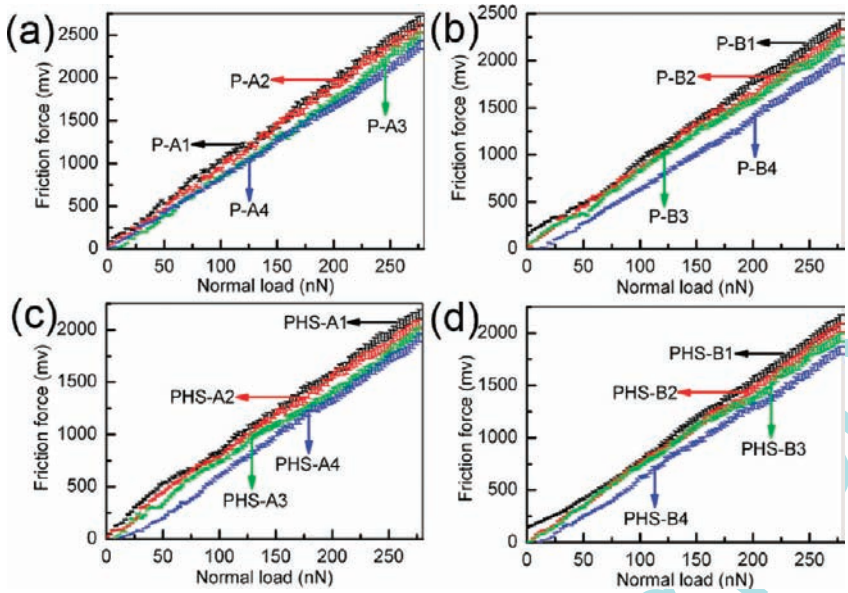

FIGURE 7. Friction forces between AFM tip and patterned surfaces with different height and fractional surface coverage, at room temperature and a relative humidity of 30−40%: (a) bare Au patterned surfaces with a height of 20 nm; (a) bare Au patterned surfaces with a height of 40 nm; (c) Au patterned surfaces with a height of 20 nm after SAMs chemical modification; (d) Au patterned surfaces with a height of 40 nm after SAMs chemical modification.

3.5. Nanotribological Properties. To investigate the nanofriction properties of the Au nanotextures surface with different height and fractional surface coverage and chemically modified with ODT SAMs, we measured the friction force versus normal load curves by AFM/FFM, and the results are shown in Figure 7. As seen from Figure 7, friction force decreased as cylindrical pillar area density and height increased, and also reduced greatly after chemical modification with ODT SAMs. Compared with the nonpatterned Au surface, the Au surface with micro/nanopillar textures greatly improved the nanotribological properties and showed lower friction forces, which was not shown in Figure 7. P-A1 showed the largest friction force and PHS-B4 showed the smallest friction force among the surfaces with micro/nanotextures investigated in this study. The friction force is given here in the form of voltage signal, which is proportional to the real friction force (37). Therefore, the results from various surfaces could be compared to each other.

The real area of contact and surface chemistry affect friction at nanoscale in dry/wet contacts strongly (1, 2, 34–36). At first, the real area of contact is dependent upon the area density and height of micro/nanopillars (1, 2, 34–36). With the same tip scan velocity, increasing of pillar height and fractional surface coverage, the number of asperities in contact is reduced greatly which lead to the real area of contact reduced and so lead to low friction force. Then, if the surface is hydrophilic, it is easy to form capillary meniscus by them or the adsorbed water molecules, which would lead to large shearing strength and higher friction (1, 2, 10). In other words, if the surface is hydrophobic, it would get the opposite result. ODT SAMs made the surface more hydrophobic lead to lower surface energy, which was also confirmed by contact angle measurement, so the friction force of PHS-B4 is the lowest among all the surfaces.

4. CONCLUSIONS

In summary, Au surfaces with micro/nanohierarchical structures were prepared via a simple, flexible and low cost template method. The effect of nanoscale roughness (pillar height and pillar fractional surface coverage) and chemical treatment (self-assembly of ODT SAMs) on the wetting properties and nanotriboloogical performance of surfaces were investigated systematically. The results show that nanotribological performance could be largely improved by designing suitable surface topography combined with hydrophobic SAMs coatings. Explanations for these phenomena are discussed in detail based on the experiments and analysis. It is expected that this paper could provide additional insight on the interesting hydrophobic phenomena by tailoring the surface topography and surface chemistry and that the principle could be applied to improve nanotribological properties of MEMS/NEMS and HDT.

Acknowledgment. Financial support for this work was provided in part by the National Natural Science Foundation of China (NSFC 20773148) and Innovative Group Foundation of NSFC (50721062).

Supporting Information Available: This material is available free of charge via the Internet at http://pubs.acs.org.

REFERENCES AND NOTES

(1) Nosonovsky, M.; Bhushan, B. *J. Phys.: Condens. Matter.* **2008**, *20*, 225009 (1−30).
(2) Nosonovsky, M.; Bhushan, B. *Curr. Opin. Colloid Interface Sci.* **2009**, *14*, 270–280.
(3) Rabinovich, Y. I.; Adler, J. J.; Ata, A.; Singh, R. K.; Moudgil, B. M. *J. Colloid Interface Sci.* **2000**, *232*, 10–16.
(4) Kira, A.; Okano, K.; Hosokawa, Y.; Naito, A.; Fuwa, K.; Yuyama, J.; Masuhara, H. *Appl. Surf. Sci.* **2009**, *255*, 7647–7651.
(5) Etsion, I. *Tribol. Lett.* **2004**, *17*, 733–737.
(6) Wang, Y.; Mo, Y. F.; Bai, M. W. *Surf. Coat. Technol.* **2008**, *203*, 137–141.
(7) Gui, J. *IEEE Trans. Magn.* **2003**, *39*, 719–721.

(8) Hsu, S. M. *Tribol. Int.* **2004**, *7*, 537–545.
(9) Bhushan, B.; Kasai, T.; Kulik, G.; Barbieri, L.; Hoffmann, P. *Ultramicroscopy* **2005**, *105*, 176–188.
(10) Zhao, W. J.; Zhu, M.; Mo, Y. F.; Bai, M. W. *Colloids. Surf., A.* **2009**, *332*, 78–82.
(11) Puukilainen, E.; Rasilainen, T.; Suvanto, M.; Pakkanen, T. A. *Langmuir* **2007**, *23*, 7263–7268.
(12) Cao, L. L.; Hu, H. H.; Gao, D. *Langmuir* **2007**, *23*, 4310–4314.
(13) Feng, X. J.; Jiang, Lei *Adv. Mater.* **2006**, *18*, 3063–3078.
(14) Ma, M. L.; Hill, R. M. *Curr. Opin. Colloid Interface Sci.* **2006**, *11*, 193–202.
(15) Marchetto, D.; Rota, A.; Calabri, L.; Gazzadi, G. C.; Menozzi, C.; Valeri, S. *Wear* **2008**, *265*, 577–582.
(16) Pettersson, U.; Staffan, J. *Tribol. Int.* **2003**, *36*, 857–864.
(17) Wakuda, M.; Yamauchi, Y.; Kanzaki, S.; Yasuda, Y. *Wear* **2003**, *254*, 356–363.
(18) Suh, A. Y.; Lee, S. C.; Polycarpou, A. A. *Tribol. Lett.* **2004**, *17*, 739–749.
(19) Laws, G. M.; Handugan, A.; Eschrich, T.; Boland, P.; Sinclair, C.; Myhajlenko, S.; Poweleit, C. D. *J. Vac. Sci. Technol., B* **2007**, *25*, 2059–2063.
(20) Xu, Q. B.; Tonks, I.; Fuerstman, M. J.; Love, J. C.; Whitesides, G. M. *Nano Lett.* **2004**, *4*, 2509–2511.
(21) Bhushan, B.; Kocha, K.; Jung, Y. C. *Soft Matter* **2008**, *4*, 1799–1804.
(22) Zheng, Z. J.; Azzaroni, O.; Zhou, F.; Huck, W. T. S. *J. Am. Chem. Soc.* **2006**, *128*, 7730–7731.
(23) Mo, Y. F.; Zhao, W. J.; Huang, D. M.; Zhao, F.; Bai, M. W. *Ultramicroscopy* **2009**, *109*, 247–252.
(24) He, B.; Chen, W.; Wang, Q. J. *Tribol. Lett.* **2008**, *31*, 187–197.
(25) Liu, H. W.; Bhushan, B. *Ultramicroscopy* **2003**, *97*, 321–340.
(26) Marchetto, D.; Rota, A.; Calabri, L.; Gazzadi, G. C.; Menozzi, C.; Valeri, S. *Wear* **2008**, *265*, 577–582.
(27) Limpoco, F. T.; Payne, J. M.; Perry, S. S. *Tribol. Lett.* **2009**, *35*, 3–7.
(28) Tsukruk, V. V.; Bliznyuk, V. N. *Langmuir* **1998**, *14*, 446–455.
(29) Mo, Y. F.; Zhao, W. J.; Zhu, M.; Bai, M. W. *Tribol. Lett.* **2008**, *32*, 143–151.
(30) Ito, E.; Konno, K.; Noh, J.; Kanai, K.; Ouchi, Y.; Seki, K.; Hara, M. *Appl. Surf. Sci.* **2005**, *244*, 584–587.
(31) Abdureyima, A.; Okudairab, K. K.; Haradac, Y.; Masudaa, S.; Aokia, M.; Sekid, K.; Ito, E.; Ueno, N. *J. Electron Spectrosc. Relat. Phenom.* **2001**, *114−116*, 371–374.
(32) Holgerson, P.; Sutherland, D. S.; Kasemod, B.; Chakarov, D. *Appl. Phys. A: Mater. Sci. Process.* **2005**, *81*, 51–56.
(33) Kim, S. H.; Asay, D. B.; Dugger, M. T. *Nanotoday* **2007**, *2*, 22–29.
(34) Zou, M.; Cai, L.; Wang, H. *Tribol. Lett.* **2006**, *21*, 25–30.
(35) Ishihara, H.; Yamagami, H.; Sumiya, T.; Okudera, M.; Inada, A.; Terada, A.; Nakamura, T. *Wear* **1994**, *172*, 65–72.
(36) Rabinovich, Y. I.; Adler, J. J.; Ata, A.; Singh, R. K.; Moudgil, B. M. *J. Colloid Interface Sci.* **2000**, *232*, 17–24.
(37) Song, S. Y.; Ren, S. L.; Wang, J. Q.; Yang, S. R.; Zhang, J. Y. *Langmuir* **2006**, *22*, 6010–6015.